Dyes and Pigments 146 (2017) 92–102

Contents lists available at ScienceDirect

Dyes and Pigments

journal homepage: www.elsevier.com/locate/dyepig

Pure space steric hindrance effect on intramolecular proton transfer in excited state and photophysics of conjugated new dyes under near-IR laser irradiation

Jihong Su [a], Yao Lu [a], Ge Ding [a], Zhenqiang Wang [a], Fanrui Huang [a], Fang Gao [a, b, *], Ziping Luo [a, b, **], Hongru Li [a, b, ***]

[a] College of Chemistry and Chemical Engineering, Chongqing University, Chongqing 400044, China
[b] National-municipal Joint Engineering Laboratory for Chemical Process Intensification and Reaction, Chongqing University, Chongqing 400044, China

ARTICLE INFO

Article history:
Received 28 April 2017
Received in revised form
27 June 2017
Accepted 27 June 2017
Available online 28 June 2017

Keywords:
Steric hindrance effect
Hydrogen bond
ESIPT
Photophysics
Conjugated dyes

ABSTRACT

This study presented a variety of new extended conjugated dyes bearing internal proton transfer segments, which were characterized with different extent of space steric hindrance. Besides, the dyes lack of proton transfer moieties were synthesized as the references. ^{1}H NMR spectra and X-ray single crystal showed presence of internal hydrogen bond in the target dyes. The study suggested that the target dyes with small or moderate space steric hindrance exhibited internal proton transfer in excited state, and thus yielded dual emission bands under one-photon and near-infrared two-photon irradiation respectively, while the dyes with heavy steric hindrance displayed quite weaker or even no intramolecular proton transfer emission in excited state. Molecular modeling to understand inhibition effect of space steric hindrance on internal proton transfer in excited state for the target dyes was further performed.

1. Introduction

Intramolecular proton transfer in excited state has been receiving intensive experimental and theoretical interests because it is an essential photoinduced process in life and nature such as in protein as well as in DNA [1–5]. It was noticed that a femtosecond or sub femtosecond ultrafast four-level cycle usually occurred in excited state intramolecular proton transfer (ESIPT) of an organic dye molecule [6,7]. For example, salicylidene methylamine underwent intramolecular proton transfer in excited state via an enol-keto phototautomerization four-level cycle mechanism ($E \rightarrow E^* \rightarrow K^* \rightarrow K \rightarrow E$, E, enol, K, keto) in an ultrafast time domain [8,9].

Hence, a normal emission band ($E^* \rightarrow E$) with its absorption and an abnormal emission band ($K^* \rightarrow K$) without its absorption of an ESIPT organic molecule could be recorded [10]. In addition, dissipated energy for getting over internal proton transfer reaction barrier in excited state gave rise to a super Stokes shift of abnormal emission band of an ESIPT organic molecule [11,12]. These unique spectroscopic properties of ESIPT organic molecules could be found application in a number of fields including bioassay, electro-optical devices as well as ions sensors [13–15]. Recently, a series of amino-type (N-H)-based hydrogen bonding organic dyes displayed dramatic substituent dependent ESIPT that presented strong application potentials as pH or acid sensors [16–20].

Thus, it is necessary to prepare larger organic dyes with ESIPT properties because they could have superior conveniences for applications comparing to small molecules. In addition, extended conjugated ESIPT dyes could be characterized with non-linear optical properties under exposure of near-infrared (near-IR) femtosecond laser, thus further yielding greater application capacities. However, energy barrier of photoinduced proton transfer in excited state could show an increase with increasing molecular size. For instance, it was thought that insertion of π segments could be a hindrance for internal proton transfer process in excited state of organic chromophores [21].

* Corresponding author. College of Chemistry and Chemical Engineering, Chongqing University, Chongqing 400044, China.
** Corresponding author. College of Chemistry and Chemical Engineering, Chongqing University, Chongqing 400044, China.
*** Corresponding author. College of Chemistry and Chemical Engineering, Chongqing University, Chongqing 400044, China.
E-mail addresses: fanggao1971@gmail.com (F. Gao), zpluo@126.com (Z. Luo), hongruli1972@gmail.com (H. Li).

http://dx.doi.org/10.1016/j.dyepig.2017.06.064
0143-7208/

It is one of main challenges for dye chemists to synthesize new enlarged organic dyes displaying intramolecular proton transfer in excited state. In order to achieve intramolecular proton transfer in excited state of enlarged dyes, some efforts have been made to develop a variety of extended conjugated dyes carrying various electron donating/withdrawing substituents [22,23]. It was revealed that internal hydrogen bond showed dependence on electron-accepting or donating nature of substituted groups, which could lead to tuning energy barrier of intramolecular proton transfer in excited state [16–20,24,25]. As a consequence, photo-tautomerization in a four-level cycle process of ESIPT could be controlled.

Internal hydrogen bond in an organic dye could be further affected by molecular geometry, and thus energy barrier of intramolecular proton transfer in excited state could be varied accordingly. Germino and his colleagues surveyed *cis*- and *trans*-conformational effect of salicylidene-5-chloroaminepyridine on intramolecular proton transfer in excited state [26]. Both Yushchenko and Krishnamoorthy groups have devoted efforts to reveal steric effect on ESIPT of heterocyclic dyes 3-hydroxyquinolones and 2-(2-hydroxyphenyl)benzimidazoles that showed strong fluorescence emission [27,28].

On the other hand, there are few studies of space steric hindrance effect on intramolecular proton transfer in excited state of organic dyes with extending π conjugation under exposure of one-photon and near-IR two-photon irradiation, respectively. Inspired by the above efforts, this study presented a range of new target dyes carrying intramolecular proton transfer segments with extension of π conjugation (**C1**, **C4** and **C7** in Scheme 1), and the corresponding reference dyes free of proton segments were prepared as well (such as **C2**, **C5** and **C8** in Scheme 1). It was shown that these target dyes were characterized with great difference in molecular geometry, in which large *trans*-diphenylethylene part in *o*- and *m*- samples **C1** and **C4** lack of electron donating/withdrawing substituents could yield pure space steric hindrance effect on internal proton transfer, while a *p*- analog **C7** could undergo intramolecular proton transfer affected by weak space steric hindrance effect (Fig. 1).

Therefore, a comprehensive experimental and theoretical investigation to show space steric hindrance effect on internal proton transfer in excited state of these target conjugated dyes under one-photon exposure and near-IR two-photon irradiation was conducted. It was observed that intramolecular proton transfer in excited state was influenced by space steric hindrance, and photophysics was affected accordingly. The results presented in this study would guide us to synthesize new ESIPT organic chromophores with extending π conjugation.

2. Experimental

2.1. Reagents and characterization

Organic solvents employed in this study were supplied by Sigma-Aldrich Corporation, which were further processed by the standard laboratory method prior to use [29]. The new studied dyes **C1**-**C9** were synthesized in our own laboratory (Scheme 1). ^{1}H and ^{13}C nuclear magnetic resonance (NMR) spectra were measured in standard NMR tubes by using tetramethylsilane (TMS) as an internal reference with Bruker 400 MHz, 500 MHz and 600 MHz apparatus at room temperature. Chemical shift multiplicities were reported as s, singlet, d, doublet and m, multiplet. FT-IR (Fourier

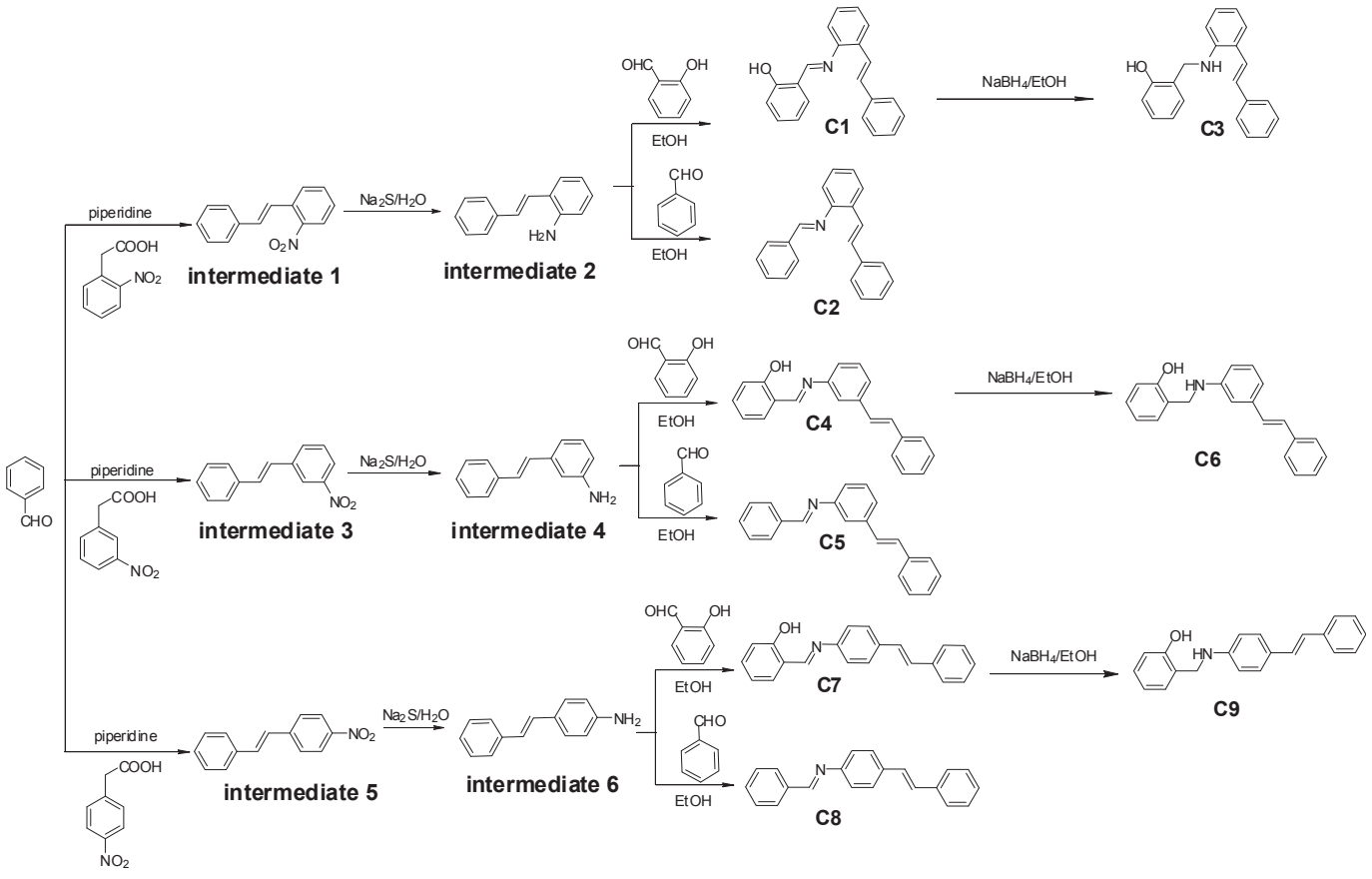

Scheme 1. Chemical structures and synthesis routes of the studied dyes in this work.

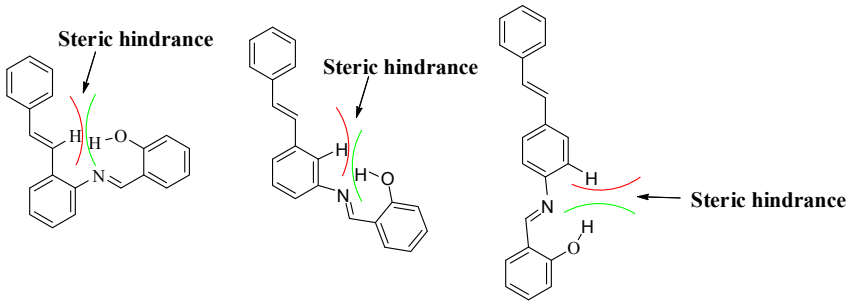

Fig. 1. Space steric hindrance showing in **C1**, **C4**, and **C7.**

transform infrared) spectra of the studied samples were recorded by KBr pellet method with Nicolet 550II IR spectrometer. All sample pellets were prepared by grinding the solid samples with dry potassium bromide (KBr) under high pressure. High resolution mass spectra (HRMS) electrospray ionization (ESI) was carried out on a UPLC-Q-ToF MS spectrometer (Waters, USA). A CE440 elemental analysis meter from Exeter Analytical Inc. was used to determine elemental analysis of the samples. The melting points of the samples were detected by a Beijing Fukai melting point apparatus.

2.2. X-ray single crystal diffraction analysis

A slow volatilization of organic solvents in NMR tube was used to incubate single crystals of the dyes. A Bruker-AXS CCD area detector equipped with diffractometer with Mo K_a ($\lambda = 0.71073$ Å) was employed to record XRD data at 298 K. A suitable single crystal was put inside a glass fiber capillary to determine structure basing on analysis by direct methods, which was refined by full-matrix least squares on F^2. All the hydrogen atoms were put in calculated positions respectively and all the non-hydrogen atoms were advanced by anisotropic temperature factors.

2.3. One-photon spectral determination and near-IR two-photon optical measurement

Spectroscopically pure solvents for UV/visible absorption and emission spectral determination measurements were provided by Sigma-Aldrich Corporation. A UV-3600 spectrophotometer from Shimadzu Corporation was utilized to measure one-photon ultraviolet/visible absorption spectra of the samples. One-photon fluorescence emission spectra of the samples were detected by Shimadzu RF-531PC spectrofluorophotonmeter. Quinine sulfate in 0.5 mol/L H_2SO_4 (Φ, 0.546) was used as the reference to determine fluorescence quantum yields of the samples [30]. The absorption in the excited wavelength was maintained below 0.1 to minimize experimental errors. Fluorescence quantum yields were calculated by Equation (1) [31]:

$$\Phi_f = \Phi_f^0 \frac{n_0^2 A^0 \int I_f(\lambda_f)\,d\lambda_f}{n^2 A \int I_f^0(\lambda_f)\,d\lambda_f} \quad (1)$$

wherein n_0 and n are refractive indices of solvents for the reference and the samples respectively, A^0 and A show absorption intensities at excitation wavelength, Φ_f and Φ_f^0 represent fluorescence quantum yields of the sample and reference molecules, and integrals show area of fluorescence bands for the reference and the samples respectively.

An Edinburgh FLS920 time-correlated single photon counting unit was utilized to measure nanosecond fluorescence lifetimes of the samples with the least-squares method in 2048 channels at room temperature, which was equipped with various light emitting diodes (excitation wavelength 330 nm and 360 nm). The optical densities at the excitation wavelengths were tuned to be lower than 0.1 to minimize experimental errors. Ultrafast fluorescence lifetimes of the samples were determined by a laser system including an intensified double photodiode array connecting with a spectrograph for time-dependent laser detection. The pump laser pulses were yielded by amplified frequency doubling directly, which were focused onto a sample cuvette and the transient spectra were registered by an ultrafast white-light continuum.

Histograms of the instrument response functions (using a LUDOX scatter) and the decays of sample solutions were recorded until they could reach 10^3 counts in the maximal channel. The acquired histograms were fitted as sums of the exponentials by using Gaussian-weighted nonlinear least squares fitting according to Marquardt–Levenberg minimization that was implemented in the software package of the detection systems. It was noticed that the fitting parameters including decay times and preexponential factors were gained by minimizing the reduced chi-square value χ^2. All curves fittings presented herein guaranteed χ^2 values lower than 1.1. Besides, the quality of the fitting results was evaluated by an additional graphical method that included plots of surfaces of the weighted residuals *versus* channel numbers.

Pumped Ti:sapphire femtosecond laser was employed to acquire near-IR two-photon excited fluorescence spectra tuning at a step of 10 nm in a range of 700–880 nm (Tsunami mode-locked, 80 MHz, <130 fs, the power ≤700 mW, Spectra-Physics Ltd.). An Ocean Optics USB2000 CCD camera with the detecting range of 180–880 nm was utilized to record TPA emission spectra. Up-conversion fluorescence method using 5×10^{-4} mol/L fluorescein in 0.1 mol/L solution of NaOH as the reference was employed to determine TPA cross-sections of the samples. Before measurement, the samples were bubbled with high purity nitrogen for 30 min to remove oxygen. TPA cross-sections of the samples were calculated by Equations (2) and (3) [32]:

$$\sigma = \frac{\sigma^{TPE}}{\Phi_F} \quad (2)$$

$$\sigma^{TPE} = \sigma_{cal}^{TPE} \frac{c_{cal}}{c} \frac{n_{cal}}{n} \frac{S}{S_{cal}} \quad (3)$$

wherein σ is two-photon absorption section, σ^{TPE} represents two-photon excited crossing section, c is concentration of reference and sample molecules, n is refractive index of the solvent, and s shows two-photon up-conversion fluorescence intensity, *cal* represents reference.

2.4. Molecular modeling

6-31G** Basis set in Gaussian 09 program package was employed to conduct molecular modeling. Geometry optimization of enol and keto tautomers in ground state (S_0) was performed by using B3LYP method based on HF (Hartree-Fock) level [33], while CIS (single-excitation configuration interaction) was used to obtain optimized geometries in the first singlet excited state (S_1) of the molecules. DFT and TD-DFT (time-dependence DFT) method at HF and CIS levels were utilized to compute the energies of optimized geometries of S_0 and S_1 respectively such as DFT//HF or TDDFT//CIS (single-point calculation//optimization method) [34]. The organic solvents were used as the media for theoretical computation.

2.5. Synthesis of the studied dyes

Synthesis routes of the studied dyes were presented in Scheme 1. All the dyes were synthesized in our laboratory firstly. Synthesis and molecular structural characterization of the intermediates were shown in Supplementary materials. Preparation details and chemical structural characterization of the studied target dyes **C1**-**C9** were described in the followings.

2.5.1. ***C1***, *2-((E)-((2-((E)-styryl)phenyl)imino)methyl)phenol*

2-Styrylaniline (0.976 g, 5 mmol) and 2-hydroxybenzaldehyde (1.220 g, 10 mmol) in 100 ml dry ethanol were added into three-necked flask. The reaction mixture was stirred at room temperature under argon protection for 12 h. After the reaction, the solvent was evaporated under vacuum. Recrystallization from ethanol and cyclohexane gave pure material as faint yellow solid (yield, 62%, m.p., 183.6–185.5 °C). ^{1}H NMR (500 MHz, $CDCl_3$-d_1) δ (ppm): 13.199 (s, -OH, 1H), 8.526 (s, N=CH, 1H), 7.720–7.702 (m, Ar-H, 1H), 7.550–7.482 (m, Ar-H, 3H), 7.400–7.368 (m, Ar-H, 2H), 7.349–7.208 (m, Ar-H, 5H), 7.106–7.051 (m, Ar-H, 2H; CH=CH, 1H), 6.978–6.921 (m, CH=CH, 1H). ^{13}C NMR (125 MHz, $CDCl_3$-d1) δ (ppm):163.488, 161.331, 146.965, 137.444, 133.477, 132.553, 130.758, 128.879, 128.804, 127.952, 127.141, 126.888, 126.653, 126.021, 124.148, 119.553, 119.303, 119.148, 117.440. FT-IR (cm^{-1}): 3438.8, 3058.3, 3025.0, 2982.2, 2923.9, 1610.4, 1589.8, 1577.3, 1559.6, 1494.4, 1476.2, 1451.3, 1279.2, 963.7, 909.7, 852.9, 757.1, 692.6. MS(ESI) *m/z*:calcd for $C_{21}H_{17}NO$ $[M+H]^+$300.13, found 300.40. Elementary analysis, Anal. Calcd for $C_{21}H_{17}NO$: C, 84.26; H, 5.72; N, 4.67. Found: C, 84.34; H, 5.65; N, 4.59.

2.5.2. ***C2***, *(E)-1-phenyl-N-(2-((E)-styryl)phenyl)methanimine*

2-Styrylaniline (0.30 g, 1.53 mmol) and benzaldehyde (0.194 g, 1.836 mmol) were added into three-necked flask containing 100 ml dry ethanol. The reaction mixture was stirred at room temperature under argon protection for 12 h. After the reaction, the solvent was evaporated under vacuum. Recrystallization from CH_2Cl_2 and cyclohexane gave pure material as faint yellow solid (yield, 48%, m.p., 178.6–180.5 °C). ^{1}H NMR (400 MHz, DMSO-d_6) δ (ppm): 8.610 (s, N=CH, 1H), 8.057–8.041 (m, Ar-H, 2H), 7.834–7.816 (d, J = 7.2 Hz, Ar-H, 1H), 7.679–7.560 (m, Ar-H, 6H), 7.417–7.354(m, Ar-H, 3H), 7.327–7.266 (m, Ar-H, 2H; CH=CH, 1H), 6.183–7.164(m, CH=CH, 1H). ^{13}C NMR (151 MHz, DMSO-d_6) δ (ppm): 161.049, 149.747, 137.770, 136.558, 132.030, 131.080, 129.868, 129.374, 129.223, 129.204, 129.158, 128.074, 126.788, 126.566, 126.180, 125.020, 119.182. FT-IR (cm^{-1}): 3432.3, 3229.0, 3080.1, 3059.8, 3023.6, 2892.2, 1943.5, 1919.6, 1886.0, 1810.8, 1623.0, 1587.7, 1575.7, 1493.5, 1476.8, 1449.9, 1372.8, 1330.8, 1310.1, 1259.9, 1220.0, 1193.1, 1167.0, 1094.6, 1072.0, 1047.7, 1024.0, 966.7, 881.8, 862.8, 760.4, 723.8, 688.4. MS(ESI) *m/z*:calcd for $C_{21}H_{17}N$ $[M+H]^+$284.14, found 284.40. Elementary analysis, Anal. Calcd for $C_{21}H_{17}N$: C, 89.02; H, 6.04; N, 4.94. Found: C, 89.13; H, 5.95; N, 5.02.

2.5.3. ***C3***, *(E)-2-(((2-styrylphenyl)amino)methyl)phenol*

2-((E)-((2-((E)-Styryl)phenyl)imino)methyl)phenol (0.2 g, 0.478 mmol) and dry ethanol 50 ml were placed into a dry round-bottomed flask, the mixture was stirred vigorously and so dium borohydride (0.17 g, 4.78 mmol) in 20 ml dry ethanol was added dropwise from a constant pressure burette at room temperature under protection of argon. The mixed solution was stirred for 2–3 h. After the reaction, the solvent was evaporated under vacuum. Recrystallization from CH_2Cl_2 and cyclohexane gave pure material as faint yellow solid (yield, 65%, m.p., 179.9–181.5 °C). ^{1}H NMR (500 MHz, DMSO-d_6) δ (ppm): 9.549 (s, -OH, 1H), 7.663–7.647 (d, J = 8.0 Hz, Ar-H, 2H), 7.539–7.507 (d, J = 16.0 Hz, CH=CH, 1H), 7.460–7.445 (d, J = 7.5 Hz, Ar-H, 1H), 7.390 (t, J = 7.75 Hz, Ar-H, 2H), 7.263–7.233 (t, J = 7.5 Hz, Ar-H, 1H), 7.152–7.138 (d, J = 7.0 Hz, Ar-H, 1H), 7.043–6.968 (m, Ar-H, 3H), 6.807–6.785 (d, J = 11.0 Hz, CH=CH, 1H) 6.721–6.692 (t, J = 7.25 Hz, Ar-H, 1H), 6.582–6.552 (t, J = 7.5 Hz, CH=CH, 1H), 6.429–6.413 (d, J = 8.0 Hz, Ar-H, 1H), 6.224 (s, -NH-, 1H), 4.309 (s, -CH_2-, 2H). ^{13}C NMR (125 MHz, DMSO-d_6) δ (ppm): 155.347, 146.240, 138.247, 129.158, 128.987, 128.487, 128.101, 127.743, 127.592, 126.954, 126.255, 126.118, 124.779, 122.514, 119.222, 116.413, 115.269, 111.245, 41.745. FT-IR (cm^{-1}): 3416.70, 3224.46, 3208.79, 3182.08, 3158.37, 3139.87, 3095.77, 3027.95, 2854.84, 1597.40, 1492.52, 1456.11, 1398.70, 1325.76, 1246.82, 1103.79, 963.64, 753.72, 692.16. MS (ESI) *m/z*:calcd for $C_{21}H_{19}NO$ $[M+H]^+$302.15, found 302.43. Elementary analysis, Anal. Calcd for $C_{21}H_{19}NO$: C, 83.70; H, 6.35; N, 4.64. Found: C, 83.82; H, 6.24; N, 4.77.

2.5.4. ***C4***, *2-((E)-((3-((E)-styryl)phenyl)imino)methyl)phenol*

Synthetic procedure and method of **C4** were the same as described in synthesis of **C1**, in which 2-styrylaniline was replaced by 3-styrylaniline. Crude product was further purified to afford the desired product as faint yellow needle solid (yield 65%, m.p., 182.3–183.4 °C). ^{1}H NMR (600 MHz, DMSO-d_6) δ (ppm): 13.106 (s, -OH, 1H), 8.997 (s, N=CH, 1H), 7.691–7.677 (d, J = 7 Hz, Ar-H, 2H), 7.644–7.632 (d, J = 6 Hz, Ar-H, 1H), 7.603–7.590 (d, J = 6.5 Hz, Ar-H, 2H), 7.445–7.431 (d, J = 7 Hz, Ar-H, 2H), 7.407–7.352 (m, Ar-H, 3H), 7.281–7.242 (m, Ar-H, 3H), 6.977–6.939 (m, CH=CH, 2H). ^{13}C NMR (151 MHz, DMSO-d_6) δ (ppm): 163.247, 160.754, 147.503, 137.455, 136.405, 133.707, 132.974, 129.162, 129.031, 128.131, 128.002, 126.941, 122.298, 119.816, 119.605, 117.034, 109.985. FT-IR (cm^{-1}): 3447.6, 3086.0, 3051.5, 3023.9, 2985.0, 2922.3, 2852.3, 2788.8, 2715.9, 2662.6, 1953.3, 1911.2, 1880.4, 1804.7, 1621.2, 1597.1, 1568.9, 1489.4, 1455.9, 1448.9, 1407.8, 1363.0, 1336.4, 1319.7, 1283.9, 1218.7, 1193.1, 1171.0, 1150.2, 1112.3, 1074.4, 1032.1, 981.1, 971.2, 955.1, 937.0, 911.9, 865.3, 848.6, 827.1, 772.9, 740.3, 720.9, 692.4, 661.8, 618.7, 557.2. MS(ESI) *m/z*:calcd for $C_{21}H_{17}NO$ $[M+H]^+$300.37, found 300.33. Elementary analysis, Anal. Calcd for $C_{21}H_{17}NO$: C, 84.25; H, 5.72; N, 4.68. Found, C, 84.31; H, 5.63; N. 4.74.

2.5.5. ***C5***, *(E)-1-Phenyl-N-(3-((E)-styryl)phenyl)methanimine*

Synthetic procedure and method of **C5** were the same as described in synthesis of **C2**, in which 2-styrylaniline was replaced by 3-styrylaniline. Crude product was further purified to afford the desired product as faint yellow needle solid (yield, 65%, m.p., 195.4–197.4 °C). ^{1}H NMR (600 MHz, DMSO-d_6) δ (ppm): 8.661 (s, N=CH, 1H), 7.933–7.920 (t, J = 3.25, Ar-H, 2H), 7.649–7.636(d, J = 6.5 Hz, Ar-H, 2H), 7.595–7.582 (d, J = 6.5 Hz, Ar-H, 2H), 7.514–7.503(d, J = 5.5 Hz, Ar-H, 3H), 7.372–7.347 (t, J = 6.25 Hz, Ar-H, 2H), 7.299–7.285 (d, J = 7 Hz, CH=CH, 2H),7.259–7.247 (t, J = 3 Hz, Ar-H, 3H). ^{13}C NMR (151 MHz, DMSO-d_6) δ (ppm):160.645, 150.953, 137.553, 136.510, 135.509, 131.913, 129.268, 129.145, 129.116, 128.454, 128.341, 128.011, 127.834, 126.871, 122.015. FT-IR (cm^{-1}): 3446.6, 3100.0, 3077.6, 3058.4, 3026.1, 2923.2, 2853.0, 2371.0, 1942.1,1869.2, 1737.4, 1622.8, 1571.9, 1498.9, 1448.0, 1365.0,

1336.0, 1313.1, 1196.7, 1165.8, 1113.3, 1072.4, 970.0, 867.5, 821.7, 746.6, 681.3, 599.7, 553.5. MS(ESI) *m/z*:calcd for $C_{21}H_{17}N$ $[M+H]^+$284.37, found 284.35. Elementary analysis, Anal. Calcd for $C_{21}H_{17}N$, C, 89.01; H, 6.05; N, 4.94. Found, C, 89.17; H, 5.89; N, 5.03.

2.5.6. ***C6****, (E)-2-(((3-styrylphenyl)amino)methyl)phenol*

Experimental procedure and method of **C6** were the same as described in synthesis of **C3**, in which 2-((E)-((2-((E)-styryl)phenyl) imino)methyl)phenol was replaced by 2-((E)-((3-((E)-styryl) phenyl)imino)methyl)phenol Crude product was further purified to afford the desired product as faint yellow solid (yield, 63%, m.p., 196.0–198.0 °C). ^{1}H NMR (600 MHz, DMSO-d_6) δ (ppm): 9.484 (s, -OH, 1H), 7.463–7.450 (d, J = 6.5 Hz, Ar-H, 2H), 7.296–7.268 (t, J = 7.0 Hz, Ar-H, 3H; CH=CH, 1H), 7.153–7.141 (d, J = 6.0 Hz, Ar-H, 2H), 7.041–7.004 (t, J = 9.25 Hz, Ar-H, 2H), 6.871–6.699 (m, Ar-H, 2H; CH=CH, 1H), 6.558–6.544 (d, J = 7.0 Hz, Ar-H, 2H), 6.240 (s, -NH-, 1H), 4.193–4.183 (d, J = 5.0 Hz, -CH_2-, 2H). ^{13}C NMR (151 MHz, DMSO-d_6) δ (ppm):155.409, 149.212, 129.437, 129.006, 128.635, 128.016, 127.960, 126.869, 126.138, 125.949, 123.232, 119.191, 115.293, 112.598. FT-IR (cm^{-1}):3271.3, 3054.9, 2921.9, 2851.2, 1818.1, 1609.6, 1590.6, 1519.8, 1487.0, 1467.7, 1384.7, 1291.5, 1247.6, 1184.0, 1104.7, 1071.8, 1036.6, 964.7, 935.5, 813.9, 748.5, 689.6, 536.9, 450.5. MS(ESI) *m/z*:calcd for $C_{21}H_{19}NO$ $[M+H]^+$302.39, found 302.39. Elementary analysis, Anal. Calcd for $C_{21}H_{17}N$: C, 83.69; H, 6.35; N, 4.65. Found, C, 83.77; H, 6.27; N. 4.72.

2.5.7. ***C7****, 2-((E)-((4-((E)-styryl)phenyl)imino)methyl)phenol*

Experimental procedure and method of **C7** were the same as described in synthesis of **C1**, in which 2-styrylaniline was replaced by 4-styrylaniline. Crude product was further purified to afford the desired product as faint yellow solid (yield, 63%, m.p. 185.0–187.5 °C). ^{1}H NMR (500 MHz, $CDCl_3$-d_1) δ (ppm): 13.292 (s, -OH, 1H), 8.654 (s, N=CH, 1H), 7.577–7.560 (d, J = 8.5 Hz, Ar-H, 2H), 7.533–7.519 (d, J = 7.0 Hz, Ar-H, 2H), 7.403–7.354 (m, Ar-H, 4H), 7.305–7.288 (d, J = 8.5 Hz, Ar-H, 2H), 7.272–7.250 (t, J = 5.5 Hz, Ar-H, 1H), 7.122 (s, CH=CH, 2H), 7.039–7.023 (d, J = 8.0 Hz, Ar-H, 1H), 6.960–6.930 (t, J = 7.5 Hz, Ar-H, 1H). ^{13}C NMR (125 MHz, $CDCl_3$-d_1) δ (ppm): 162.119, 161.376, 147.695, 137.695, 136.447, 133.338, 132.443, 129.125, 128.916, 127.967, 127.698, 126.726, 121.786, 119.462, 119.286, 117.459. FT-IR (cm^{-1}): 3448.3, 3102.8, 3077.6, 3052.3, 3024.1, 2987.9, 2924.0, 2853.2, 2788.8, 2710.3, 1621.3, 1591.8, 1569.3, 1489.7, 1455.9, 1448.7, 1284.0, 826.8, 750.9, 739.8, 691.7. MS (ESI) *m/z*:calcd for $C_{21}H_{17}NO$ $[M+H]^+$300.13, found 300.44. Elementary analysis, Anal. Calcd for $C_{21}H_{17}NO$: C, 84.26; H, 5.72; N, 4.68. Found: C, 84.32; H, 5.79; N, 4.59.

2.5.8. ***C8****, (E)-1-phenyl-N-(4-((E)-styryl)phenyl)methanimine*

Experimental procedure and method of **C8** were the same as described in synthesis of **C2**, in which 2-styrylaniline was replaced by 4-styrylaniline. Crude product was further purified to afford the desired product as faint yellow solid (yield, 60%, m.p., 179.9–180.5 °C). ^{1}H NMR (600 MHz, DMSO-d_6) δ (ppm):8.672 (s, N=CH-, 1H), 7.943–7.931 (t, J = 3.6 Hz, Ar-H, 2H), 7.660–7.646 (d, J = 8.4 Hz, Ar-H, 2H), 7.605–7.593 (d, J = 7.2 Hz, Ar-H, 2H), 7.525–7.514 (d, J = 6.6 Hz, Ar-H, 3H), 7.383–7.358 (t, J = 7.5 Hz, Ar-H, 3H), 7.309–7.296 (d, J = 7.8 Hz, CH=CH, 2H), 7.270–7.262 (d, J = 4.8 Hz, Ar-H, 2H). ^{13}C NMR (151 MHz, DMSO-d_6) δ (ppm): 160.642, 150.949, 137.551, 136.509, 135.507, 131.911, 129.266, 129.143, 129.116, 128.450, 128.339, 128.011, 127.832, 126.869, 122.014. FT-IR (cm^{-1}): 3237.18, 3208.17, 3194.63, 3157.26, 3125.13, 3093.42. 1447.87, 1403.71, 963.39, 867.85, 821.73, 746.11, 690.05. MS(ESI) *m/z*:calcd for $C_{21}H_{17}N$ $[M+H]^+$284.14, found 284.43. Elementary analysis, Anal. Calcd for $C_{21}H_{17}N$: C, 89.02; H, 6.04; N, 4.91. Found: C, 89.17; H, 5.95; N, 5.11.

2.5.9. ***C9****, (E)-2-(((4-styrylphenyl)amino)methyl)phenol*

Synthesis of **C9** followed essentially the same procedure as described that of **C3**, in which 2-((E)-((2-((E)-styryl)phenyl)imino) methyl)phenol was replaced by 2-((E)-((4-((E)-styryl)phenyl) imino)methyl)phenol. The product was further purified to give pure material as faint yellow solid (yield, 52%, m.p., 162.6–163.8 °C). ^{1}H NMR (600 MHz, DMSO-d_6) δ (ppm): 9.500 (s, -OH, 1H), 7.475–7.462 (d, J = 7.8 Hz, Ar-H, 2H), 7.307–7.294 (t, J = 5.2 Hz, Ar-H, 4H), 7.165–7.153 (d, J = 4.8 Hz, Ar-H, 2H), 7.053–7.026 (d, J = 10.8 Hz, CH=CH, 2H), 6.883–6.855 (d, J = 11.2 Hz, Ar-H, 1H), 6.815–6.802 (d, J = 7.8 Hz, Ar-H, 1H), 6.723–6.699 (t, J = 7.2 Hz, Ar-H, 1H), 6.570–6.556 (d, J = 8.4 Hz, Ar-H, 2H), 6.264–6.244 (t, J = 6.0 Hz, -NH-, 1H), 4.206–4.196 (d, J = 6.0 Hz, -CH_2, 2H). ^{13}C NMR (151 MHz, DMSO-d_6) δ (ppm): 160.157, 153.961, 143.128, 134.185, 133.758, 133.381, 132.767, 132.710, 131.620, 130.888, 130.695, 129.819, 127.977, 123.939, 120.039, 117.344, 46.353. FT-IR (cm^{-1}): 3429.22, 3270.66, 3055.60, 3020.98, 2923.91, 2889.29, 2847.91, 1609.28, 1588.58, 1519.35, 1484.74, 1401.96, 1290.96, 1249.58, 1180.35, 965.88, 813.87, 744.64, 689.33.MS(ESI) *m/z*:calcd for $C_{21}H_{19}NO$ $[M+H]^+$302.15, found 302.43. Elementary analysis, Anal. Calcd for $C_{21}H_{19}NO$: C, 83.70; H, 6.35; N, 4.64. Found: C, 84.83; H, 6.26; N, 4.72.

3. Results and discussion

3.1. Internal hydrogen bond based on ^{1}H NMR spectra

Hydrogen bond showed a remarkable influence on ^{1}H NMR chemical shift of its relevant hydrogen atoms. Representative ^{1}H NMR spectra of the target **C1** and its references **C2** and **C3** in DMSO-d_6 were shown in Fig. 2. ^{1}H NMR spectral peak of phenolic hydroxy group in **C1** shifted to more down-magnetic field comparing to that of **C3** (**C1**, 13.199 ppm *versus* **C3**, 9.549 ppm). In addition, ^{1}H NMR chemical shift of HC=N in **C1** moved to more up-magnetic field than that of **C2** (**C1**, 8.526 ppm *versus* **C2**, 8.610 ppm). It was observed that ^{1}H NMR chemical shift phenolic hydroxy group in equal molar **C2**/phenol mixture was almost identical to that of phenol (Fig. S1).

It was further discovered that ^{1}H NMR spectral peak of hydroxy group in **C1** shifted to much lower magnetic field with respect to that phenol (**C1**, 13.199 ppm, phenol, 9.350 ppm). As a matter of the fact, the other target dyes **C4** and **C7** also showed similar ^{1}H NMR spectral phenomena as **C1**. The results indicated that intramolecular hydrogen bond in the target dyes could give rise to a decrease of electron cloud density around hydrogen atom of phenolic hydroxy group, and thus shielding effect could be lowered. As a result, chemical shift of ^{1}H NMR peak of hydroxy group in the target dyes showed a shift to low magnetic field.

3.2. Intramolecular hydrogen bond analysis basing on X-ray single crystal diffraction

X-ray single crystal diffraction analysis provided further experimental evidence of internal hydrogen bond. Single crystals of the target dyes were prepared by slow evaporation of mixed organic solvents. The dihedral angles between phenolic hydroxy and imino groups in the target dyes were particularly analyzed by X-ray single crystal diffraction. Fig. 3 showed that HC=CH and HC=N double bands in **C1** and **C7** presented good *trans*-configuration. In addition, there were small dihedral angles around HC=CH and HC=N bonds, suggesting coplanar nature of the conjugated π parts in the target dyes (such as **C1**, ∠C8-N1-C1-C2, 2.34°; ∠C13-C14-C15-C16, 2.72°, Fig. 2), which were favorable for formation of intramolecular hydrogen bond. X-ray single crystal diffraction analysis suggested that internal hydrogen bond between phenolic hydroxy and imino

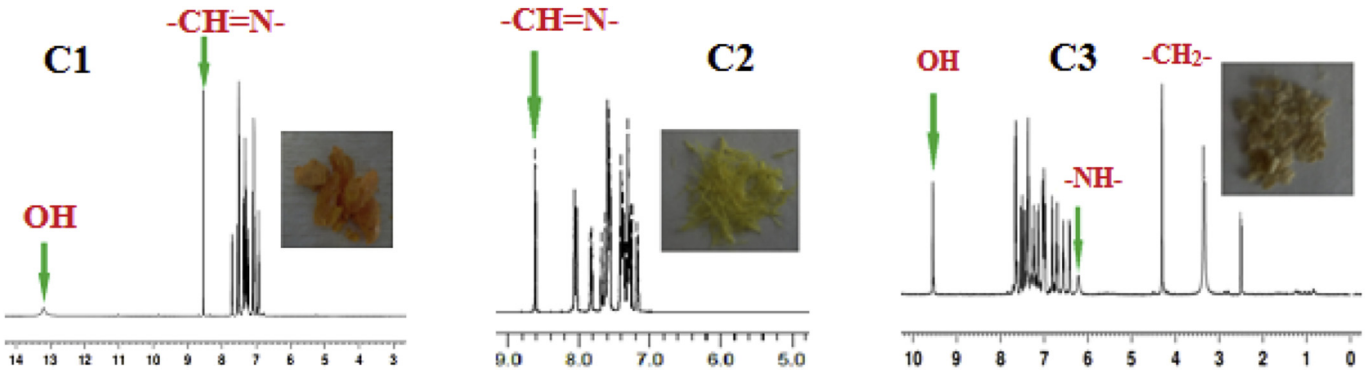

Fig. 2. ^{1}H NMR spectra of **C1**, **C2** and **C3** in DMSO-d_6.

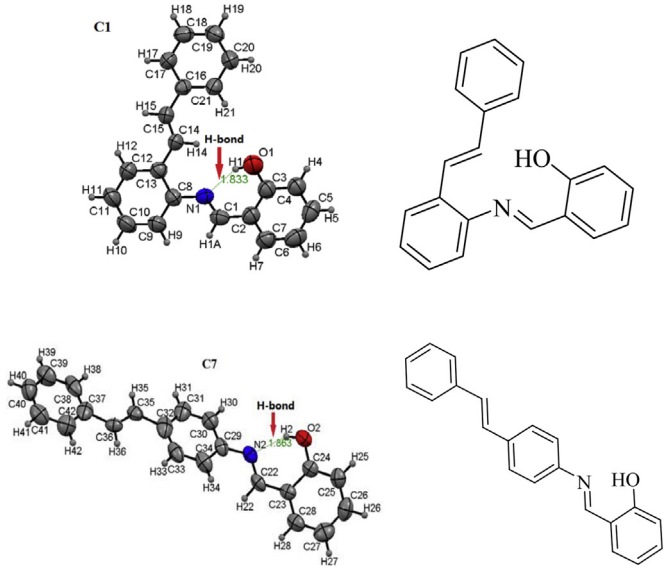

Fig. 3. ORTEP drawings of **C1** and **C7** with 30% possibility of thermal ellipsoids.

groups in **C1** and **C7** existed.

3.3. One-photon UV/visible absorption spectra of the studied dyes

UV/visible absorption spectrum of an organic molecule reflected its structural feature in ground state. Representative UV/visible absorption spectra of **C1**, **C4** and **C7** in DMF and 1,4-dioxane were presented in Fig. 4. UV/visible absorption parameters of **C1**, **C4** and **C7** in various organic solvents were given in Table 1.

Owing to electron withdrawing effect of *o*-hydroxy-phenyl-imino part segment, internal charge transfer from diphenyl-ethylene part to *o*-hydroxy-phenyl-imino segment in **C1**, **C4** and **C7** could exist, which could be further shown by electron cloud density distribution in HOMO and LUMO orbitals in the ground state. Thus, UV/visible absorption spectra of these target dyes could be characterized by (π, π) transition with intramolecular charge transfer nature.

It was found that UV/visible absorption spectra of **C1** and **C7** were presented as a mirror-image-like relationship (Fig. 4). The second absorption band of **C1** was shown as a shoulder (at about 350 nm) and its first absorption band (at approximate 300 nm) was primary, while the first absorption band of **C7** was presented as a shoulder and its second absorption band was prevailing. The first absorption band could be ascribed to normal (π, π) transition, and the second long absorption band could be assigned to intramolecular charge transfer. The results indicated that ortho substitution in **C1** could decrease entire molecular internal charge transfer in ground state due to space steric hindrance, while para substitution in **C7** increased intramolecular charge transfer without steric hindrance. In addition, meta substitution in **C4** with moderate space steric hindrance produced a remarkably separated dual absorption bands.

It was further found that the reference **C2**, **C5** and **C8** exhibited remarkable the long-wavelength absorption band with an approximate 360 nm peak in various solvents (Fig. S2). This could be mainly due to lack of phenolic hydroxy group, leading to an increase in structural planarity, and thus internal charge transfer was guaranteed. While to **C3**, **C6** and **C9**, amine group increased intramolecular charge transfer in entire molecules. Accordingly, two absorption peaks of **C3**, **C6** and **C9** could be observed as well.

In a word, the first absorption band peaked around 300 nm of the target dyes could be assigned to whole molecular (π, π) transition, while the second absorption band centered approximate 350 nm could be yielded by intramolecular charge transfer of entire molecular frameworks. It was necessary to point out that the presence of internal hydrogen bond could give rise to increase of intramolecular charge transfer of the target dyes **C4** and **C7**, which could result in obvious bathochromic shift of the absorption maxima with respect to those of the reference dyes respectively (such as **C7**, 365 nm, **C8**, 352 nm, **C9**, 331 nm).

3.4. One-photon steady and transient emission spectra of the studied dyes

Intramolecular hydrogen bond in ground state of **C1**, **C4** and **C7** suggested that intramolecular proton transfer in excited state could occur. One-photon fluorescence emission spectra of the targets and the references were determined for analyzing internal proton transfer in excited state. The fluorescence spectral parameters of **C1**, **C4** and **C7** in various solvents were given in Table 1. The representative fluorescence spectra of **C1**, **C4** and **C7** in DMF and 1,4-dioxane were presented in Fig. 5.

First, the fluorescence spectral difference between **C1** and **C7** was concentrated. It was found that **C1** showed single fluorescence band peaked at 450 nm in most of organic solvents. Only in a few protic solvents such as n-propanol (Fig. S3), it displayed an emission shoulder around 530 nm attaching to the primary band peaked at 454 nm. In contrast, **C7** exhibited well-separated fluorescence bands in various solvents which included the first emission band with the maximal peak at 435 nm, and the second emission band with the emission maximum at 530 nm.

The corresponding references such as **C5** and **C8** showed single

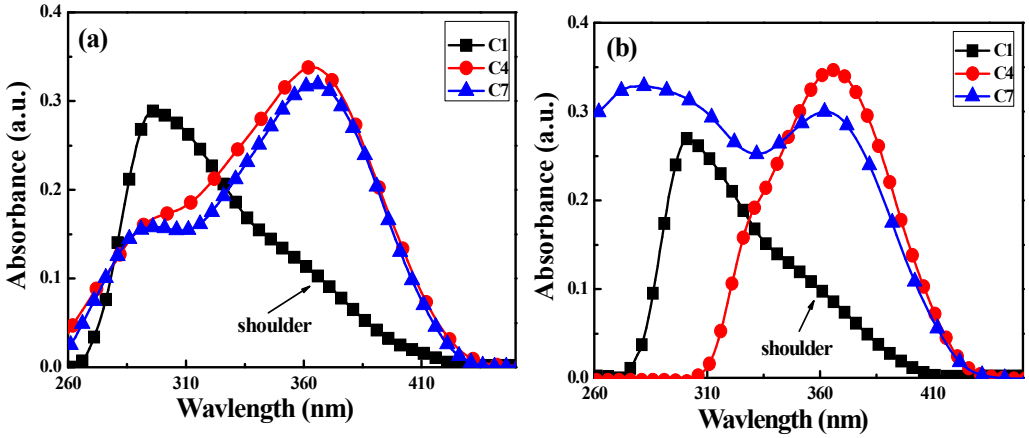

Fig. 4. One-photon UV/visible absorption spectra of **C1**, **C4** and **C7** in DMF (a) and in 1,4-dioxane (b), C, 1×10^{-5} mol/L.

Table 1
One-photon spectral parameters of **C1**, **C4** and **C7** in various solvents, $\lambda_{a,max}$: the absorption maximum (nm), ε_{max}: the maximal molar extinction coefficient (10^5 cm^{-1} mol^{-1} L), $\lambda_{f,max}$: the emission maximum (nm), Φ: the fluorescence quantum yield.

Solvents	C1				C4				C7			
	$\lambda_{a,max}$	ε_{max}	$\lambda_{f,max}$	Φ	$\lambda_{a,max}$	ε_{max}	$\lambda_{f,max}$	Φ	$\lambda_{a,max}$	ε_{max}	$\lambda_{f,max}$	Φ
1,4-dioxane	297	0.268	435	0.00917	364	0.310	529	0.00716	365	0.349	561	0.00920
CH_2Cl_2	297	0.294	436	0.00829	346	0.426	533	0.00316	363	0.349	536	0.00570
Acetonitrile	298	0.281	429	0.0250	361	0.408	525	0.0504	361	0.295	534	0.00704
DMSO	297	0.377	481	0.0694	369	0.272	528	0.0101	368	0.389	531	0.00914
DMF	295	0.288	465	0.00902	362	0.337	532	0.00390	364	0.366	531	0.00827
Ethanol	295	0.225	450	0.00785	360	0.312	527	0.00585	361	0.272	530	0.00904

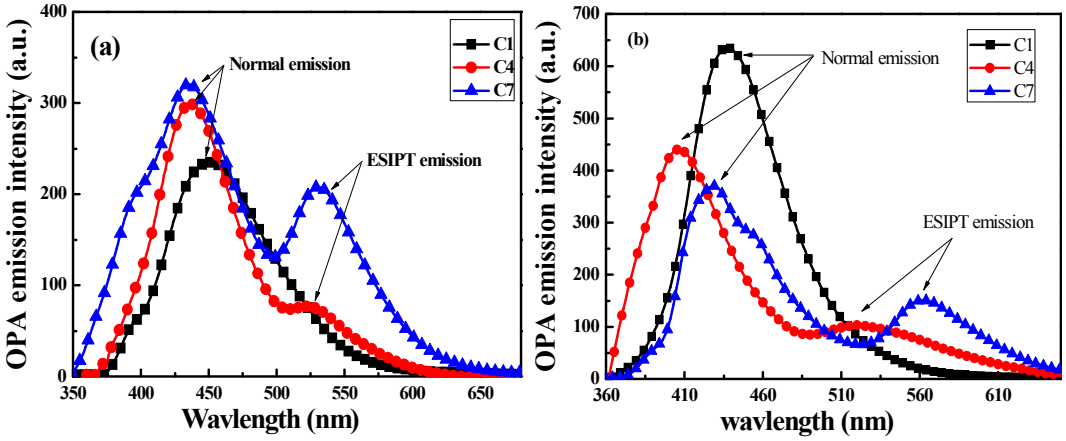

Fig. 5. One-photon emission spectra of **C1**, **C4** and **C7** in DMF (a) and in 1, 4-dioxane (b), Ex: 350 nm, C, 1×10^{-5} mol/L.

emission band in various solvents (Fig. S4). The emission maxima of these references were characterized with normal Stokes shifts (about 81 nm for **C5**), which were also similar as the maximal emission wavelengths of the first fluorescence bands of **C4** and **C7**. In addition, the emission peaks of the references were close to the emission maxima of **C1** in various solvents.

It was observed that the emission peaks of the second fluorescence bands of **C4** and **C7** shifted to much longer wavelengths in various solvents (such as **C7**, 531 nm in DMF), which displayed huge Stokes shifts (such as 167 nm in DMF for **C7**). It was also noticed that the emission shoulder peaks of **C1** (appearance only in a few modest polar solvents) were close to the emission maxima of the second fluorescence bands of **C4** and **C7**. As a matter of fact, **C4** and **C7** showed similar well-separated double emission bands in solid state as well as in polymer matrix, while in contrast, the corresponding references displayed similar single fluorescence bond.

It was further discovered that the maximal peaks of **C1** displayed close fluorescence lifetimes as the first emission bands of **C4** and **C7** respectively (such as in DMF, **C1**, 1.42 ns, **C4**, 1.35 ns, **C7**, 1.26 ns, typically shown in Fig. S5). However, the fluorescence lifetimes of the second emission bands of **C4** and **C7** were shorter than those of the first emission bands (such as in DMF, **C4**, 0.34 ns, **C7**, 0.23 ns).

Hence, the results suggested that the first emission bands **C4** and **C7** were produced by the tautomer enol* to enol decay, while the second emission bands were yielded by the decay of tautomer keto* to keto. The fluorescence emission of **C1** was primarily

ascribed to the excited enol decay, and the fluorescence emission of the reference dyes such as **C2**, **C5** and **C8** was effectively the same as $S_0 \rightarrow S_1$ absorption spectral characteristics.

It was further found that the emission intensity ratios of the keto emission band to that of the normal emission band (I_{K^*}/I_{E^*}) of **C7** were larger than **C4** in various solvents (such as in DMF, **C7**, 0.524, **C4**, 0.201), suggesting that **C7** could undergo ESIPT more efficiently than **C4**. It was also shown that **C7** and **C4** displayed a more competitive keto emission in DMF than in 1,4-dioxane. This could be due to greater internal charge transfer in DMF, leading to a more active hydroxy group. As a result, ESIPT was more pronounced in DMF.

Accordingly, the excited energies of **C4** and **C7** were dissipated by internal proton transfer, which diminished fluorescence quantum yields comparing to the corresponding reference molecules **C5** and **C8** (such as **C4**, 0.00390, **C5**, 0.00449, in DMF, Table S1). It was noticed that the fluorescence quantum yields of the target dyes **C1**, **C4** and **C7** and the reference dyes **C2**, **C5** and **C8** showed low fluorescence emission, which could be mainly due to rotation and isomerization of free imino group leading to nonradiative deactivation [35,36].

Because the fluorescence emission of **C4** and **C7** were consisted of the normal emission and ESIPT emission, the fluorescence quantum yields were the sum of the enol fluorescence quantum yield and the keto fluorescence quantum yield, as shown in the following Equation (4) [37]

$$\Phi_{f\,(sum)} = \Phi_{f\,(enol)} + \Phi_{f\,(keto)} \quad (4)$$

wherein $\Phi_{f\,(sum)}$ is the total fluorescence quantum yield of the dyes, $\Phi_{f\,(enol)}$ represents the total fluorescence quantum yields of enol forms, $\Phi_{f\,(keto)}$ shows the total fluorescence quantum yields of keto forms.

Since the absorption was produced by tautomer enol to enol*, the ratio of the integrated area of the first emission band (normal enol band) and the second normal emission band (keto band) to those of the total emission represented the percent of enol emission or keto emission to the total fluorescence quantum yield respectively. Thus, the fluorescence quantum yields of the tautomers enol and keto forms of **C4** and **C7** could be acquired respectively.

Therefore, we could further calculate radiative transition constants (k_r) and non-radiative transition constants of enol decay and keto decay according to the following Equation (5) [38]:

$$k_r = \Phi_f/\tau_f \quad (5)$$

$$k_{nr} = (1 - \Phi_f)/\tau_f \quad (6)$$

wherein Φ_f is the fluorescence quantum yield, and τ_f shows the lifetime determined at the maximal emission wavelength.

Radiative transition rates and non-radiative transition constants (s^{-1}) of the tautomers enol and keto in excited state of **C1**, **C4** and **C7** were given in Table 2. It was given that enol **C1** displayed larger radiative transition rate of than enol **C4** and **C7,** respectively, demonstrating that normal emission decay was more competitive in excited state of **C1**. In addition, **C7** exhibited greater radiative transition rate of keto form than **C4**, suggesting that keto emission decay was stronger in excited state of **C7**.

It was noticed that nonradiative transition rate of enol **C1** was smaller than that of **C4** and **C7,** respectively, which further suggested that the normal emission decay could be stronger in excited state of **C1**. It was found that keto **C4** exhibited greater nonradiative transition rate than keto **C7**, which indicated that keto emission decay was stronger in excited state of **C7**. As a consequence, a more remarkable dual-emission band of **C7** was observed. The data also showed that **C7** produced larger radiative transition rate of keto tautomer band in DMF than in 1,4-dioxane, thus it presented more competitive ESIPT in DMF.

Table 2
Radiative transition rates and non-radiative transition constants (s^{-1}) of the tautomers enol and keto in excited state of **C1**, **C4** and **C7** in DMF and 1,4-dioxane.

Dyes		Solvents	
		DMF	1,4-dioxane
C1	$\Phi_{f\,(enol)}$	0.00902	0.00917
	$\tau_{f\,(enol)} \times 10^{-9}$ (s)	1.42	2.55
	$k_{r\,(enol)} \times 10^{9}$ (s^{-1})	0.00635	0.00360
	$k_{nr\,(enol)} \times 10^{9}$ (s^{-1})	0.698	0.389
C4	$\Phi_{f\,(enol)}$	0.00329	0.00547
	$\tau_{f\,(enol)} \times 10^{-9}$ (s)	1.35	2.45
	$k_{r\,(enol)} \times 10^{9}$ (s^{-1})	0.00244	0.00223
	$k_{nr\,(enol)} \times 10^{9}$ (s^{-1})	0.738	0.406
	$\Phi_{f\,(keto)}$	0.000610	0.00169
	$\tau_{f\,(keto)} \times 10^{-9}$ (s)	0.34	0.47
	$k_{r\,(keto)} \times 10^{9}$ (s^{-1})	0.00179	0.00360
	$k_{nr\,(keto)} \times 10^{9}$ (s^{-1})	2.923	2.124
C7	$\Phi_{f\,(enol)}$	0.00538	0.00650
	$\tau_{f\,(enol)} \times 10^{-9}$ (s)	1.26	2.33
	$k_{r\,(enol)} \times 10^{9}$ (s^{-1})	0.00421	0.00279
	$k_{nr\,(enol)} \times 10^{9}$ (s^{-1})	0.789	0.426
	$\Phi_{f\,(keto)}$	0.00289	0.00270
	$\tau_{f\,(keto)} \times 10^{-9}$ (s)	0.23	0.36
	$k_{r\,(keto)} \times 10^{9}$ (s^{-1})	0.0126	0.00751
	$k_{nr\,(keto)} \times 10^{9}$ (s^{-1})	0.987	2.770

3.5. Intramolecular proton transfer in excited state basing on two-photon absorption under near-IR laser irradiation

Femtosecond Ti:sapphire near-IR laser was utilized to measure two-photon absorption (TPA) nature of the targets and the references. TPA fluorescence difference between **C1** and **C7** was particularly analyzed. It was found that **C1** and **C7** showed a mirror-image-like TPA emission spectral shape under near-IR 720 nm femtosecond laser irradiation (Fig. 6). **C1** displayed a primary TPA fluorescence emission band peaked at 430 nm and a secondary TPA emission band with a 550 nm peak. While **C7** displayed a major TPA fluorescence emission band peaked at 550 nm and a minor TPA emission band with a 430 nm maximum. **C4** displayed a similar TPA emission shape as **C7**.

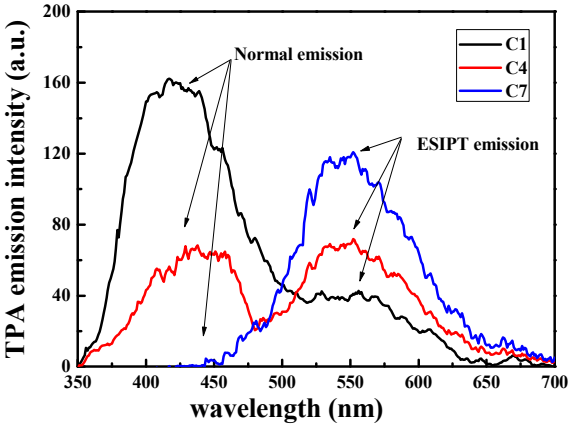

Fig. 6. Near-IR two-photo emission spectra of **C1**, **C4** and **C7** under 720 nm femtosecond laser irradiation.

In contrast, the references such as **C2**, **C5** and **C8** showed single TPA fluorescence bands with the emission maximum at about 430 nm (Fig. S6), which were close to the peak wavelength of the first TPA emission bands of **C1**, **C4** and **C7**. In addition, the fluorescence lifetimes of the first TPA emission bands and the second emission bands of **C4** and **C7** were almost same as those of the first OPA ones, respectively.

Hence, it was concluded that the first TPA emission bands of the targets were yielded by excited enol decay under near-IR femtosecond laser, while the second TPA emission bands were produced by excited keto decay. On the other hand, the ratio of TPA fluorescence emission intensity of the second band to the first band showed an order as **C7**>**C4**>**C1**, which suggested that space steric hindrance inhibited intramolecular proton transfer in excited state under two-photon irradiation as well.

It was necessary to point out that TPA ESIPT emission of the target dyes were more competitive in excite state under near-IR laser exposure. Ratios of the second band to the first band in TPA fluorescence spectra of the target dyes became more remarkable than those in one-photon emission spectra, which could be mainly due to that femtosecond pulsed near-IR laser matched well time domain of intramolecular proton transfer in excited state. As a consequence, internal proton transfer could be a competitive pathway to deactivate excited state of the target dyes under near-IR femtosecond laser irradiation.

TPA cross-sections of the studied dyes were further determined based on TPA fluorescent methods. The results showed that the target dyes displayed larger near-IR TPA cross-sections than the corresponding reference dyes (such as **C7**, 47.2 GM, **C8**, 3.4 GM, **C9**, 1.5 GM in DMF, 1 GM, 10^{-50} $cms^{-1}photon^{-1}$). It was considered that intramolecular hydrogen bond in the target molecules could favor intramolecular charge transfer and molecular aggregation [39], and thus TPA absorption sections of the target dyes increased. We would point out that **C4** and **C7** showed larger near-IR TPA cross-sections than **C1** (such as **C1**, 20.7 GM, **C4**, 33.6 GM, **C7**, 47.2 GM in DMF), which indicated that space steric hindrance played a negative role in two-photon absorption cross section due to restraint of π extension. This further explained why **C4** and **C7** showed more competitive near-IR TPA-based ESIPT emission than **C1**.

3.6. Molecular geometry optimization

3.6.1. Geometrical parameters

Molecular geometry optimization of the target dyes was carried out to find out fundamental reason of space steric hindrance effect on ESIPT. The calculation showed that the target **C1**, **C4** and **C7** yielded transition states (TS) of enol-keto tautomerization in the ground and excited states respectively. In contrast, owing to free of hydroxy group, the reference **C2**, **C5** and **C8** could not produce keto transition forms. In addition, E-K transition forms of the reference **C3**, **C6** and **C9** could not be obtained either, because no suitable proton accepter was contained. As a consequence, it was impossible to undergo internal proton transfer in the ground and excited states of the reference dyes, while it was possible to process intramolecular proton transfer in the target ones.

Table S2 showed that distances of H-O and H-N (in ortho-hydroxy-phenyl-imino part) in TS states of the target dyes in S_0 and S_1 states were between those of tautomers forms (such as H-O in S_1, **C7**, E, 0.957 Å, TS, 1.250 Å, K, 1.817 Å). This meant that intramolecular proton transfer could be required to be through an energy-barrier pathway. In addition, the distances of O-N in transition states of the target dyes were much shorter than those of E and K forms in both S_0 and S_1 states, which suggested that transition state possessed the strongest internal hydrogen bond strength than E and K forms in both S_0 and S_1 states of the target dyes. It was inferred that internal proton transfer of the target dyes could occur as long as the energy barrier could be overcome.

Dihedral angles of ∠CCCN in the *o*-hydroxy-phenyl-imino part of the target dyes was also computed (Table S3). Small dihedral angles in S_0 reflected coplanarity in *ortho*-hydoxy-phenyl-imino part in the targets (such as **C7**, $\angle C_1$-C_2-C_3-N_1, 0.754°). It was further found that coplanarity in *o*-hydoxy-phenyl-imino part were more remarkable in S_1 (such as **C7**, $\angle C_1$-C_2-C_3-N_1, 0.540°), which favored internal proton transfer. It was shown that coplanarity in S_1 of **C7** was greater than the excited **C1** and **C4** (such as **C7**, $\angle C_1$-C_2-C_3-N_1, 0.754°; **C1**, $\angle C_1$-C_2-C_3-N_1, -1.317°; **C4**, $\angle C_1$-C_2-C_3-N_1, -0.780° in S_1), indicating that ESIPT could be more possible in **C7**.

It was observed that the distance of N-H in **C1** was the longest, while it was the shortest in **C7** among all the excited state target dyes (such as **C1**, 2.092 Å, **C7**, 1.851 Å). In contrast, the distance of O-H in **C1** was the smallest, while it was the longest in **C7** among excited target dyes (such as **C1**, 0.945 Å, **C7**, 0.957 Å). This showed that internal proton transfer tunnel in excited state could follow as **C1**>**C4**>**C7**.

Dihedral angles of ∠CNCC attached to diphenylethylene part of the target dyes were further emphasized. A large torsion of ∠CNCC in S_0 of **C1**, **C4** and **C7** indicated that internal proton transfer in ground state could be very difficult (such as **C1**, $\angle C_3$-N_1-C_4-C_5, 44.916°, **C4**, $\angle C_3$-N_1-C_4-C_5, 41.695°). In contrast, smaller torsion of ∠CNCC in S_1 state of **C1**, **C4** and **C7** suggested more possibility of intramolecular proton transfer in excited state than that in ground state of the target dyes (such as **C1**, $\angle C_3$-N_1-C_4-C_5, 0.596°, **C4**, 43.318°). It was also found that dihedral angle of $\angle C_6$-C_7-C_8-C_9 in **C7** tended be close to zero degree in excited state, which further suggested that **C7** possessed a larger ability to undergo internal proton transfer in S_1.

We also noticed that the dihedral angle of ∠COHN in the excited state of **C1** was much larger than that of **C4** and **C7** respectively (**C1**, $\angle C_1$-O_1-H_1-N_1, 35.251°, **C4**, $\angle C_1$-O_1-H_1-N_1, 0.3445°, **C7**, $\angle C_1$-O_1-H_1-N_1, 1.302°). This indicated that a quasi six-membered ring (N-C-C-C-O-H) formed by internal hydrogen bond in **C7** could be more coplanar in excited state. As a consequence, **C1** could be more difficult to undergo intramolecular proton transfer in excite state than **C4** and **C7**.

3.6.2. Frontier orbitals, Mulliken atomic charge and dipole moment

The target and reference dyes displayed π-symmetric characteristic of HOMO and LUMO orbitals in the ground and excited states (Fig. S7). In HOMOs of the target dyes, electron cloud density was mainly distributed in diphenylethylene part, while less electron cloud density distribution was located at *o*-hydroxy-phenyl-imino segment (Fig. S7). However, as the target dyes were excited from HOMO to LUMO orbitals, electron cloud density distribution moved to *o*-hydorx-phenyl-imino part. Hence, a larger charge density distribution in proton transfer segment part could be a drive for ESIPT of the target dyes.

It was found that as E was excited to E^*, part of negative charge was transferred from hydroxy to imino group in the target dyes. As a consequence, negative charge in proton donor (O atom) of the target dyes decreased from E to E^* (such as **C1**, in S_0, -0.671 e, S_1, -0.669 e in Table S4), which suggested less basicity and more acidity of hydroxy group in excited state. It was further found that **C7** showed the greatest decrease of negative charge in O atom. In contrast, the negative charge in proton receptor (N atom) of the target dyes increased (such as **C1**, S_0, -0.699 e, S_1, -0.741 e), which reflected less acidity and more basicity. It was observed that N atom of **C7** exhibited more negative charge and greater variations than that in **C1** while it was excited from S_0 to S_1. This suggested that it was more easily to undergo internal proton transfer in excited state of **C7**.

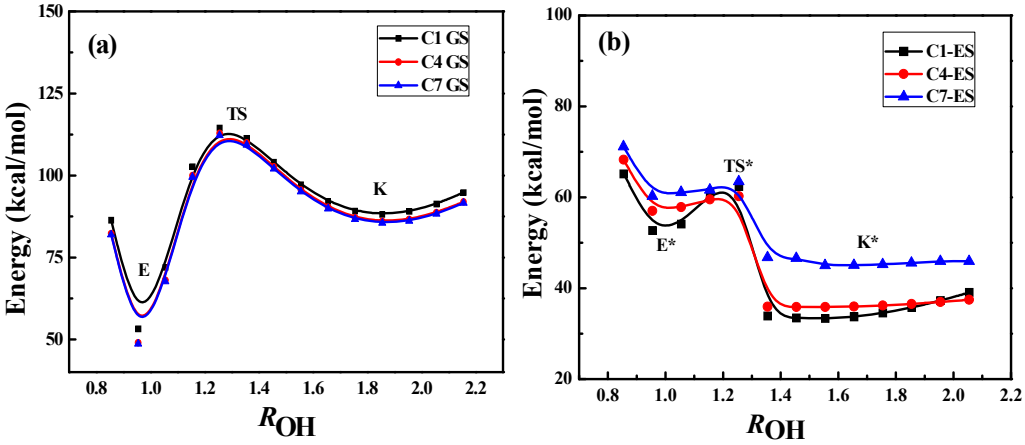

Fig. 7. Proton transfer reaction potential energy curves relaxed along the O-H distance in ground (a) and the first single excited state (b) for **C1**, **C4** and **C7.**

Charge changes of the atoms were indications of dipole moment changes of the entire target dyes. The computation showed that the dipole moments of the transition states were between the enol and keto tautomers in the ground and excited states of the target molecules (such as **C1**, enol, 2.537 D, TS, 3.695 D, keto, 3.904 D, in ground state), suggesting the tautomerization of the target dyes could be required to get over an energy barrier channel. The reduced dipole moments of the tautomers in excited state suggested that it was more easily to undergo intramolecular proton transfer in S_1 than in S_0 (such as enol of **C7**, S_0, 2.595 D, S_1, 2.527 D in Table S5). In particular, tautomer enol **C1** showed a least decrease in dipole moment as it was excited from S_0 to S_1 than enol **C4** and **C7,** respectively, which suggested a least reactivity in S_1 state of **C1** and a largest difficulty of ESIPT.

3.6.3. Energy barriers of tautomerization of in S_0 and S_1 states

Potential curves of intramolecular proton transfer in S_0 and S_1 states of **C1**, **C4** and **C7** were computed respectively. Fig. 7 showed the typical plots of potential curves of intramolecular proton transfer as a function of O-H distance in S_0 and S_1 states of **C1**, **C4** and **C7**. It was shown that energy barrier of intramolecular proton transfer in S_0 and S_1 of the target dyes existed, respectively.

The plots showed that E form was more stable in ground state and K form was more stable in excited state to these target dyes. Hence, intramolecular proton transfer in excited state of the target molecules could be possible. The further calculation showed that direct energy barrier of internal proton transfer (E→K, shown as ΔEd) was much larger in S_0 than in S_1 states, suggesting that it was quite harder to undergo internal proton transfer in S_0 (such as to **C7**, S_0, 15.204 kcal/mol, S_1, 3.191 kcal/mol, Table S6). In contrast, the reverse reaction energy barrier in ground state (K→E, shown as ΔEr) was much lower than that in excited state of the target dyes (such as to **C7**, S_0, 6.390 kcal/mol, S_1, 18.451 kcal/mol). This further demonstrated that occurrence of ground state intramolecular proton transfer (GSIPT, E→K→E) was more difficult than that of ESIPT (E→E^*→K^*→K→E). In addition, small ΔEr in ground state implied that it was could be easy to proceed reverse internal proton transfer (namely from K→E) to the target dyes, which in turn was favorable for four-level cycle process of ESIPT.

We further noticed that direct energy barrier (ΔEd) of enol-keto tautomerization in **C7** was smaller than that of **C1** and **C4** in excited state (**C1**, 9.703 kcal/mol, **C4**, 3.244 kcal/mol, **C7**, 3.191 kcal/mol). Furthermore, the reverse energy barrier (ΔEr) of keto-enol tautomerization in **C7** was lower than that of **C1** and **C4** in ground state (**C1**, 6.591 kcal/mol, **C4**, 6.424 kcal/mol, **C7**, 6.390 kcal/mol). Hence, **C7** could possess a larger possibility to undergo ESIPT than **C1** and **C4**. In addition, **C4** showed a smaller direct energy barrier (ΔEd) of enol-keto tautomerization than **C1** in exited state, and it displayed a lower reverse energy barrier (ΔEr) of keto-enol tautomerization than **C1** in ground state. As a consequence, **C4** could have a larger possibility to process internal proton transfer than **C1** in excited state.

4. Conclusions

To be closing, this study presented a series of conjugated organic dyes containing proton transfer segments used as the targets as well as the reference ones free of proton transfer parts. Intramolecular hydrogen bond in the target dyes was demonstrated by ^{1}H NMR spectra and X-ray single crystal diffraction. The studies demonstrated that the target dyes with large space steric hindrance underwent negligible ESIPT emission under one-photon irradiation, while the target ones with light space steric hindrance showed remarkable keto fluorescence. Although all the target dyes showed well-separated keto bands under near-IR femtosecond laser exposure, the keto emission competition deceased with increasing space steric hindrance. In contrast, there were no signs of ESIPT for the reference dyes due to lack of proton donors or acceptors under one-photon exposure and near-IR femtosecond two-photon irradiation. The molecular geometry optimization showed that the target dyes with smaller space steric hindrance possessed a variety of superior advantages over the ones carrying larger steric hindrance such as better coplanarity as well as smaller potential energy barrier of phototautomerization, and as a consequence, a more competitive ESIPT could occur.

Acknowledgements

The authors thank financial support from Natural Science Foundation of Chongqing (CSTC2012jjB50007 and CSTC2010BB0216). H. L. appreciates China Postdoctoral Science Foundation for financial supporting (Grant Nos. 22012T50762 & 2011M501388). The authors also thank Key Laboratory of Photochemical Conversion and Optoelectronic Materials, TIPC, Chinese Academy of Sciences for laser measurement. We greatly thank Analytic and Testing Center of Chongqing University for various determinations.

Appendix A. Supplementary data

Supplementary data related to this article can be found at http://dx.doi.org/10.1016/j.dyepig.2017.06.064.

References

[1] Zhang H, Feng W, Feng G. A simple and readily available fluorescent turn-on probe for cysteine detection and bioimaging in living cells. Dyes Pigments 2017;139:73–8.
[2] Ghodbane A, Fellows WB, Bright JR, Ghosh D, Saffon N, Tolbert LM, et al. Effects of the benzoxazole group on green fluorescent protein chromophore crystal structure and solid state photophysics. J Mater. Chem C 2016;4:2793–801.
[3] Padalkar VS, Seki S. Excited-state intramolecular proton-transfer (ESIPT)-inspired solid state emitters. Chem Soc Rev 2016;45:169–202.
[4] Chen KY, Cheng YM, Lai CH, Hsu CC, Ho ML, Lee GH, et al. Ortho green fluorescence protein synthetic chromophore; excited-state intramolecular proton transfer via a seven-membered-ring hydrogen-bonding system. J Am Chem Soc 2007;129:4534–5.
[5] Xu S, Shao Y, Ma K, Cui Q, Liu G, Wu F, et al. Fluorescence light-up recognition of DNA nucleotide based on selective abasic site binding of an excited-state intramolecular proton transfer probe. Analyst 2011;136:4480–5.
[6] Stasyuk AJ, Chen YT, Chen CL, Wu PJ, Chou PT. A new class of N-H excited-state intramolecular proton transfer (ESIPT) molecules bearing localized zwitterionic tautomers. Phys Chem Chem Phys 2016;18:24428–36.
[7] Malakar P, Modak D, Prasad E. Pure white light emission from organic molecules using solvent induced selective self-assembly. Chem Commu 2016;52:4309–12.
[8] Jankowska J, Barbatti M, Sadlej J, Sobolewski AL. Tailoring the Schiff base photoswitching—a non-adiabatic molecular dynamics study of substituent effect on excited state proton transfer. Phys Chem Chem Phys 2017;19:5318–25.
[9] Zhao L, Liu J, Zhou P. New insight into the photoisomerization process of the salicylidene methylamine under vacuum. J Phys Chem A 2016;120:7419–26.
[10] Kim D, Kwon JE, Park SY. Is color-specific photoswitching in dual-color fluorescence systems possible? Manipulating intermolecular energy transfer among two different fluorophores and one photoswitch. Adv Opt Mater 2016;4:790–7.
[11] Mutai T, Ohkawa T, Shono H, Araki K. The development of aryl-substituted 2-phenylimidazo [1, 2-a] pyridines (PIP) with various colors of excited-state intramolecular proton transfer (ESIPT) luminescence in the solid state. J Mater. Chem C 2016;4:3599–606.
[12] Tang L, Zheng Z, Zhong K, Bian YA. 2, 5-diaryl-1, 3, 4-oxadiazole-based fluorescent probe for rapid and highly selective recognition of hydrogen sulfide with a large Stokes shift through switching on ESIPT. Tetrahedron Lett 2016;57:1361–4.
[13] Cui L, Baek Y, Lee S, Kwon N, Yoon J. An AIE and ESIPT based kinetically resolved fluorescent probe for biothiols. J Mater. Chem C 2016;4:2909–14.
[14] Li B, Tang G, Zhou L, Wu D, Lan J, Zhou L, et al. Unexpected sole enol-form emission of 2-(2′-hydroxyphenyl) oxazoles for highly efficient deep-blue-emitting organic electroluminescent devices. Adv Funct Mater 2017;27:1605245–53.
[15] Jin X, Sun X, Di X, Zhang X, Huang H, Liu J, et al. Novel fluorescent ESIPT probe based on flavone for nitroxyl in aqueous solution and serum. Sensors Actuators B Chem 2016;224:209–16.
[16] Zhou J, Outlaw VK, Townsend CA, Bragg AE. Quenching of pH-responsive luminescence of a benzoindolizine sensor by an ultrafast hydrogen shift. Chem Eur J 2016;22:15212–5.
[17] Outlaw VK, Zhou J, Bragg AE, Townsend CA. Unusual blue-shifted acid-responsive photoluminescence behavior in 6-amino-8-cyanobenzo [1, 2-b] indolizines. RSC Adv 2016;6:61249–53.
[18] Tseng HW, Lin TC, Chen CL, Lin TC, Chen YA, Liu JQ, et al. A new class of N–H proton transfer molecules: wide tautomer emission tuning from 590 nm to 770 nm via a facile, single site amino derivatization in 10-aminobenzo [h] quinoline. Chem Commu 2015;51:16099–102.
[19] Chen CL, Tseng HW, Chen YA, Liu JQ, Chao CM, Liu KM, et al. Insight into the amino-type excited-state intramolecular proton transfer cycle using N-tosyl derivatives of 2-(2-aminophenyl)benzothiazole. J Phys Chem A 2016;120:1020–8.
[20] Tseng HW, Liu JQ, Chen YA, Chao CM, Liu KM, Chen CL, et al. Harnessing excited-state intramolecular proton-transfer reaction via a series of amino-type hydrogen-bonding molecules. J Phys Chem Lett 2015;6:1477–86.
[21] Zhao J, Ji S, Chen Y, Guo H, Yang P. Excited state intramolecular proton transfer (ESIPT): from principal photophysics to the development of new chromophores and applications in fluorescent molecular probes and luminescent materials. Phys Chem Chem Phys 2012;14:8803–17.
[22] Gong Y, Wang Z, Zhang S, Luo Z, Gao F, Li H. New ESIPT-inspired photostabilizers of two-photon absorption coumarin-benzotriazole dyads: from experiments to molecular modeling. Indus Eng Chem Res 2016;55:5223–30.
[23] Jagadesan P, Whittemore T, Beirl T, Turro C, McGrier PL. Excited-state intramolecular proton-transfer properties of three tris(N-Salicylideneaniline)-based chromophores with extended conjugation. Chem Eur J 2016;23:917–25.
[24] Ping GY, Liang YH. Theoretical studies of conjugation and substituent effect on intramolecular proton transfer in the ground and excited states. Chem Phys 2006;322:382–6.
[25] Wang R, Liu D, Xu K, Li J. Substituent and solvent effects on excited state intramolecular proton transfer in novel 2-(2′-hydroxyphenyl) benzothiazole derivatives. J Photochem Photobio Part A Chem 2009;205:61–9.
[26] Germino JC, Barboza CA, Quites FJ, Vazquez PAM, Atvars TDZ. Dual emissions of salicylidene-5-chloroaminepyridine due to excited state intramolecular proton transfer: dynamic photophysical and theoretical studies. J Phys Chem C 2015;119:27666–75.
[27] Yushchenko DA, Shvadchak VV, Klymchenko AS, Duportail G, Pivovarenko VG, Mély Y. Steric control of the excited-state intramolecular proton transfer in 3-hydroxyquinolones: steady-state and time-resolved fluorescence study. J Phys Chem A 2007;111:8986–92.
[28] Behera SK, Sadhuragiri G, Elumalai P, Sathiyendiran M, Krishnamoorthy G. Exclusive excited state intramolecular proton transfer from a 2-(2′-hydroxyphenyl) benzimidazole derivative. RSC Adv 2016;6:59708–17.
[29] Perrin DD, Armarego WLF, Perrin DR. Purification of laboratory chemicals. New York, NY: Pergamon; 1966.
[30] Grabolle M, Spieles M, Lesnyak V, Gaponik N, Eychmüller A, Resch-Genger U. Determination of the fluorescence quantum yield of quantum dots: suitable procedures and achievable uncertainties. Anal Chem 2009;81:6285–94.
[31] Maus M, Rettig W, Bonafoux D, Lapouyade R. Photoinduced intramolecular charge transfer in a series of differently twisted donor– acceptor biphenyls as revealed by fluorescence. J Phys Chem A 1999;103:3388–401.
[32] Xu C, Webb WW. Measurement of two-photon excitation cross sections of molecular fluorophores with data from 690 to 1050 nm. JOSA B 1996;13:481–91.
[33] Ping GY, Liang YH, Cao CZ. Intramolecular proton or hydrogen-atom transfer in the ground-and excited-states of 2-hydroxybenzophenone: a theoretical study. Chem Phys 2005;315:297–302.
[34] Liang YH, Ping GY. Theoretical studies on structure, energetic and intramolecular proton transfer of alkannin. Chem Phys Lett 2007;438:173–7.
[35] Wu JS, Liu WM, Zhuang XQ, Wang F, Wang PF, Tao SL, et al. Fluorescence turn on of coumarin derivatives by metal cations: a new signaling mechanism based on C=N isomerization. Org Lett 2007;9:33–6.
[36] Jang YK, Nam UC, Kwon HL, Hwang IH, Kim C. A selective colorimetric and fluorescent chemosensor based-on naphthol for detection of Al^{3+} and Cu^{2+}. Dyes Pigments 2013;99:6–13.
[37] Ding G, Lu Y, Gong Y, Ma L, Luo Z, Zhang S, et al. New AB2 type two-photon absorption dyes for well-separated dual-emission: molecular preorganization based approach to photophysical properties. Tetrahedron 2016;72:3040–56.
[38] Becker RS. Theory and interpretation of fluorescence and phosphorescence. New York: Wiley-Interscience; 1969.
[39] Zeng L, Chen S, Xia T, Zhong C, Liu Z. Designing two-photon fluorescent probes based on the target-induced enhancement of the absorption cross-section. Chem Commu 2014;50:11139–42.